Abnormal Muscle Spindle Innervation and Large-Fiber Neuropathy in Diabetic Mice

Karra A. Muller,[1] Janelle M. Ryals,[1] Eva L. Feldman,[2] and Douglas E. Wright[1]

OBJECTIVE—Large-fiber diabetic polyneuropathy (DPN) leads to balance and gait abnormalities, placing patients at risk for falls. Large sensory axons innervating muscle spindles provide feedback for balance and gait and, when damaged, can cause altered sensorimotor function. This study aimed to determine whether symptoms of large-fiber DPN in type 1 and type 2 diabetic mouse models are related to alterations in muscle spindle innervation. In addition, diabetic mice were treated with insulin to assess whether sensorimotor and spindle deficits were reversible.

RESEARCH DESIGN AND METHODS—Behavioral assessments were performed in untreated and treated streptozotocin (STZ)-injected C57BL/6 mice to quantitate diabetes-induced deficits in balance and gait. Quantification of Ia axon innervation of spindles was carried out using immunohistochemistry and confocal microscopy on STZ-injected C57BL/6 and *db/db* mice.

RESULTS—STZ-injected C57BL/6 mice displayed significant and progressive sensorimotor dysfunction. Analysis of Ia innervation patterns of diabetic C57BL/6 spindles revealed a range of abnormalities suggestive of Ia axon degeneration and/or regeneration. The multiple abnormal Ia fiber morphologies resulted in substantial variability in axonal width and inter-rotational distance (IRD). Likewise, *db/db* mice displayed significant variability in their IRDs compared with db^+ mice, suggesting that damage to Ia axons occurs in both type 1 and type 2 diabetes models. Insulin treatment improved behavioral deficits and restored Ia fiber innervation in comparison with nondiabetic mice.

CONCLUSIONS—Similar to small fibers, Ia axons are vulnerable to diabetes, and their damage may contribute to balance and gait deficits. In addition, these studies provide a novel method to assay therapeutic interventions designed for diabetes-induced large-fiber dysfunction. ***Diabetes*** **57:1693–1701, 2008**

Estimates from the Centers for Disease Control and Prevention suggest that 60–70% of diabetic patients develop neuropathy. In addition, diabetes is the leading cause of neuropathy in the U.S. and Western countries (1). Sensorimotor diabetic polyneuropathy (DPN) affects both large and small sensory afferent nerve fibers. The majority of research focuses on small-fiber neuropathy leading to increased or decreased pain and temperature sensations (2–5). Consequently, there is a shortage of animal model research exploring large-fiber DPN, which can cause deficits in lower-limb proprioception, decreased tactile sensitivity and vibration sense, and incoordination due to balance abnormalities (1,6).

The sensorimotor deficits resulting from large-fiber DPN, while sometimes subtle in nature, can lead to significant impairment. Numerous human studies report that patients with DPN are at increased risk for falls due to decreased postural control, altered gait and balance, and increased body sway (7–9). The underlying neurologic mechanisms involved in large-fiber DPN remain poorly understood. It has been hypothesized that large-fiber DPN instability could be caused by altered sensorimotor function, specifically damaged group Ia and II sensory afferent fibers in muscle spindles (10).

Muscle spindles found within skeletal muscle are rapidly adapting sensorimotor receptors. Spindles in mice are surrounded by extrafusal muscle fibers and consist of bag and chain intrafusal fibers. Three subtypes of nerves innervate the intrafusal fibers: group Ia and II large sensory axons and γ motor axons. Muscle spindles are involved in many sensorimotor behaviors such as the regulation of proprioception, balance, gait, and the postural response (11,12), and spindle damage can lead to deficits such as incoordination. Multiple studies in humans reported morphologic changes to the aging muscle spindle that could contribute to increased falls and ataxia seen in the elderly (13,14). In rodents, Egr3-null mutant mice have muscle spindle degeneration postnatally, resulting in an ataxic gait (15). Therefore, it is plausible that symptoms of large-fiber DPN could result from damage to muscle spindle large afferent fibers.

Here, we examined streptozotocin (STZ)-induced type 1 and leptin receptor–null mutant type 2 diabetic mouse models for evidence of large-fiber DPN. Our results suggest the presence of STZ-induced large-fiber DPN using a behavioral test of sensorimotor function, and muscle spindle quantification reveals Ia afferent morphologic changes in the width of the axon and the inter-rotational distance (IRD) of annulospiral endings. The leptin receptor–null mutant mice also displayed aberrant muscle spindle morphology similar to that seen in type 1 diabetic mice. Importantly, insulin treatment in STZ-induced diabetic mice improved behavioral performance and normalized Ia axon morphology in muscle spindles. These novel results provide evidence that disrupted muscle spindle innervation in both type 1 and type 2 diabetic models may be involved, at least in part, in the sensorimotor deficits displayed in STZ-induced DPN.

From the [1]Department of Anatomy and Cell Biology, University of Kansas Medical Center, Kansas City, Kansas; and the [2]Department of Neurology, University of Michigan, Ann Arbor, Michigan.

Corresponding author: Douglas Wright, PhD, Department of Anatomy and Cell Biology, University of Kansas Medical Center, Kansas City, KS 66160. E-mail: dwright@kumc.edu.

Received for publication 7 January 2008 and accepted in revised form 21 March 2008.

Published ahead of print at http://diabetes.diabetesjournals.org on 24 March 2008. DOI: 10.2337/db08-0022.

DPN, diabetic polyneuropathy; IRD, inter-rotational distance; MNCV, motor nerve conduction velocity; SNCV, sensory nerve conduction velocity; STZ, streptozotocin.

TABLE 1
Body weight and blood glucose concentrations in C57BL/6, leptin receptor-null mutant, and insulin-treated mice

	Early		Terminal	
	Weight (g)	Blood glucose (mmol/l)	Weight (g)	Blood glucose (mmol/l)
Nondiabetic C57BL/6	23 ± 0.8	6.1 ± 0.49	28 ± 0.4	6.6 ± 0.55
Diabetic C57BL/6	19 ± 0.5*	18.9 ± 1.40**	22 ± 1.0*	29.1 ± 1.18**
db$^+$	NA	NA	28 ± 0.9	8.0 ± 0.64
db/db	NA	NA	51 ± 1.5*	28.7 ± 2.29*
Diabetic + sham pellets	19 ± 0.3	17.8 ± 1.04	21 ± 0.9	20.2 ± 0.51
Diabetic + insulin pellets	21 ± 0.7	17.0 ± 0.82	26 ± 0.7*	13.1 ± 2.33*

Data are means ± SEM. Weight and blood glucose levels measured at an early timepoint (1 week post-STZ for C57BL/6 mice or 15 weeks of age for leptin receptor null mutant mice) and the final timepoint (10 weeks post-STZ or 24 weeks of age). *$P < 0.05$ vs. nondiabetic, *db*$^+$ mice, or diabetic + sham pellets; **$P < 0.0001$ vs. nondiabetic or *db*$^+$ mice. NA, not available.

RESEARCH DESIGN AND METHODS

Male C57BL/6 mice were purchased at 7 weeks of age from Charles River (Wilmington, MA) and housed two mice per cage on a 12:12-h light/dark cycle in the animal facility at the University of Kansas Medical Center under pathogen-free conditions. Male *db/db* mice (strain BKS.Cg-*m*$^{+/+}$Lepr^{db}/J, stock number 000642, background strain C57BLKS/J) were purchased from Jackson Laboratories (Bar Harbor, ME) and were housed at the University of Michigan under pathogen-free conditions on a 12:12-h light/dark cycle. A breeding colony was established, and mice were genotyped after birth. All animals had free access to water and mouse diet (C57BL/6 mice: Harlan Teklad 8,604, 4% kcal derived from fat; *db/db* and *db*$^+$ mice: LabDiet 5001, 12% kcal derived from fat), and use was in accordance with National Institutes of Health guidelines and approved by the University of Kansas Medical Center Animal Care and Use Committee or the University of Michigan Committee on the Care and Use of Animals, respectively.

STZ-injected C57BL/6 mice. Diabetes was induced in 8-week-old C57BL/6 mice ($n = 10$) by a single intraperitoneal injection of STZ (Sigma, St. Louis, MO) at 180 mg/kg body wt (16). Nondiabetic mice ($n = 8$) were injected with 400 μl vehicle buffer. Hyperglycemia and diabetes was defined as a blood glucose level >16 mmol/l (~288 mg/dl). Weight and tail vein blood glucose levels were measured using glucose diagnostic reagents (Sigma) and analyzed using a two-way repeated-measures ANOVA with Fisher's protected least significant difference post hoc test.

Insulin administration. In a separate group of animals, insulin pellets were administered to five STZ-induced C57BL/6 diabetic mice, while six diabetic and six nondiabetic mice received sham palmitic acid pellets. Insulin replacement therapy began 6 weeks post-STZ injection via LinBit sustained release insulin pellets (13 ± 2 mg each, 0.1 unit/24 h; LinShin Canada, Scarborough, ON, Canada) implanted subcutaneously in the dorsal skin (two pellets for the first 20 g body wt and an additional pellet for every additional 5 g body wt). All pellets remained in the mice for 4 weeks, and an additional insulin pellet was added if blood glucose levels failed to drop to <16 mmol/l after 1 week. Weight and blood glucose levels were measured and analyzed as described above.

***db/db* mice.** Diabetes was confirmed in *db/db* mice at 8 weeks of age. Immunohistochemical analysis and quantification of muscle spindles were performed on medial gastrocnemius muscles from 24-week-old homozygous (*db/db*; $n = 3$) and heterozygous (*db*$^+$; $n = 3$) leptin receptor–null mutant mice.

Beam walk. Mice were trained during weeks 2 and 3 post-STZ to traverse a 1 m–long wooden beam with a diameter of 1.2 cm (adapted from 17,18). The animals were recorded for three trials per session on weeks 3, 5, and 10 post-STZ injection. The behavior task was recorded using a digital video camera. A footslip was counted if either the left or right hindpaw slipped off the beam. The number of footslips/mouse was averaged, and the data were analyzed using a two-way repeated-measures ANOVA with Fisher's protected least significant difference post hoc test.

Footprinting. Footprinting was used as previously described in Taylor et al. (18). The rear paws of C57BL/6 mice were inked, and mice walked along a 6 × 70 cm track lined with paper at 10 weeks post-STZ. For each tracking, three to five prints were analyzed for step length, toe spread (distance between toes 1–5), intermediate toe spread (inter-toe spread; distance between toes 2–4), and print length. Means were calculated for each animal and analyzed using unpaired *t* tests.

Grid walk. The grid-walk apparatus consisted of an elevated 1.1-cm wire grid that was 20 × 35 cm, adapted from Onyszchuk et al. (19). Animals were recorded with a digital video camera for 5 min while walking on the grid at 10 weeks post-STZ injection. Hindpaw steps and the number of hindpaw foot faults, or slips, were counted. The percent of slips was calculated for each animal (hindpaw slips/total hindpaw steps × 100) and analyzed using unpaired *t* tests.

Rotorod. The rotorod (AccuRotor Rota Rod; AccuScan Instruments, Columbus, OH) was used as described in Taylor et al. (18). STZ-induced C57BL/6 mice were tested on the rotorod at a constant speed of 12 rpm for three trials at 9 weeks' post-STZ injection. The latency of the mice to remain on the rotorod (in seconds) was recorded, and mean latencies were analyzed using unpaired *t* tests.

Nerve conduction velocity. Nerve conduction velocities were recorded in STZ-induced diabetic ($n = 6$) and nondiabetic ($n = 6$) mice at 10 weeks post-STZ injection according to Stevens et al. (20). Body temperature was monitored with a rectal probe and maintained at 37°C. Motor nerve conduction velocities (MNCVs) were obtained by measuring compound muscle action potentials using supramaximal stimulation (9.9 mA) distally at the ankle and proximally at the sciatic notch. Recordings were obtained from the first interosseous muscle. Sensory nerve conduction velocity (SNCV) was recorded behind the medial malleolus with a 0.5-ms square wave pulse using the smallest current to elicit a response (~2.4 mA), stimulating at the digital nerve of the second toe. Diabetic and nondiabetic nerve conduction velocities were analyzed by unpaired *t* tests.

Immunohistochemistry. C57BL/6 mice were killed at 10 weeks post-STZ and *db/db* and *db*$^+$ mice at 24 weeks of age. Unfixed medial gastrocnemius muscles were dissected, frozen, sectioned in 50-μm longitudinal serial sections, and mounted on Superfrost Plus slides (Fisher Scientific, Chicago, IL). Immunohistochemistry was performed according to Taylor et al. (17). Intrafusal bag fibers were visualized using a mouse anti–slow-tonic myosin heavy chain antibody (S46, 1:50; generous gift from Dr. Frank Stockdale, Stanford, CA). Sensory axons were visualized using a rabbit anti-neurofilament H antibody (NFH, 1:500; Chemicon, Temecula, CA). The NFH primary antibody used (#AB1991) is not affected by neurofilament phosphorylation.

Muscle spindle quantification. Fluorescent digital images were acquired using a Nikon Digital Eclipse C1si confocal microscope. Approximately two to six muscle spindles per muscle were imaged for spindle innervation quantification. Digital Z-stack images of spindles were transferred to Nikon Imaging Software-Elements (NIS-Elements; Melville, NY). For each spindle the mean width of three or more axonal rotations and the mean IRD (the space in between the axonal rotations) between three or more rotations were calculated and recorded by a blinded observer using NIS-Elements. Mean axonal width and mean IRD were analyzed using unpaired *t* tests.

RESULTS

One week following STZ injection, C57BL/6 mice displayed characteristic symptoms of diabetes, including polydipsia and polyuria. Diabetic mice had significantly reduced weight gain and significantly higher blood glucose levels as early as 1 week post-STZ, which persisted through the study until week 10 (Table 1). In addition, *db/db* mice displayed significantly higher body weights and blood glucose levels from week 15 through the terminal week 24 (Table 1). Lastly, diabetic mice after treatment with insulin had significantly higher weights and significantly lower blood glucose levels than diabetic mice with sham pellets (Table 1).

The number of hindpaw slips as mice crossed the beam-walk apparatus was used to access sensorimotor ability. For a slip to be counted, the foot had to lose

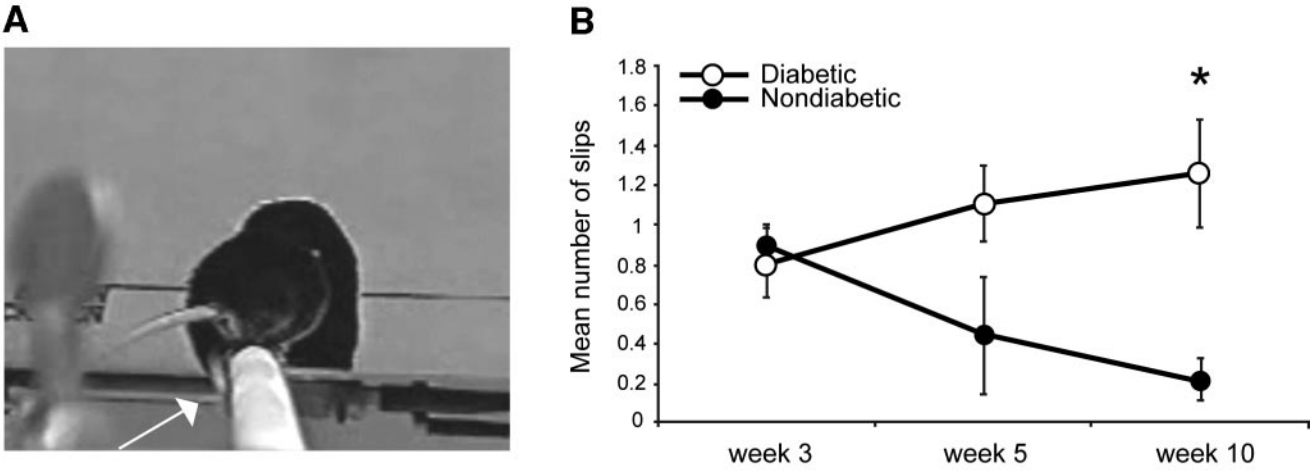

FIG. 1. Sensorimotor evaluation on beam-walk in STZ-treated C57BL/6 diabetic mice. *A*: Photograph of a nondiabetic C57BL/6 mouse performing the beam-walk task. White arrow denotes a slip of the left hindpaw. *B*: Quantification of mean hindpaw footslips for diabetic (n = 10) and nondiabetic (n = 3) mice at 3, 5, and 10 weeks' post-STZ injection. Diabetic mice had significantly more slips at 10 weeks post-STZ. Data are presented as means ± SEM. *P < 0.05 vs. nondiabetic mice.

contact with the balance beam with the leg extended (Fig. 1*A*). At week 3 post-STZ injection, there was no significant difference between the mean number of slips that were counted for nondiabetic (mean ± SEM, 0.9 ± 0.11) and diabetic (0.8 ± 0.18) mice (Fig. 1*B*). Likewise, at 5 weeks post-STZ, there was no significant difference in footslips between nondiabetic (0.4 ± 0.29) and diabetic (1.1 ± 0.19) mice; however, a trend related to poorer performance in diabetic than nondiabetic mice was apparent (Fig. 1*B*). After 10 weeks of hyperglycemia, the diabetic mice displayed a significantly greater number of footslips (1.3 ± 0.27) than nondiabetic (0.2 ± 0.11; $P < 0.05$) mice (Fig. 1*B*). These results suggest that STZ-induced diabetes in C57BL/6 mice leads to a sensorimotor dysfunction that is detectable by the beam-walk apparatus.

To examine additional measures of sensorimotor function, footprinting, grid walk, and rotorod tests were performed in STZ-induced diabetic mice. Interestingly, none of the tasks were sensitive enough to detect the sensorimotor deficits displayed during the beam-walk tests. All footprinting parameters were not different between nondiabetic and diabetic mice (Table 2). In addition, the percentage of grid-walk slips and rotorod latencies of diabetic mice were not significantly different from those of nondiabetic mice (Table 2). These results suggest that the beam-walk apparatus is the most sensitive test to expose sensorimotor dysfunction in STZ-induced diabetes.

Conduction velocities of motor and sensory nerve fibers were assessed in nondiabetic and diabetic C57BL/6 mice. Diabetic mice had significantly slower MNCV than nondiabetic mice (49.5 ± 2.2 vs. 58.7 ± 2.4 m/s; $P < 0.05$). In comparison, there was no difference in SNCV between diabetic and nondiabetic mice (32.6 ± 1.1 vs. 31.7 ± 0.9 m/s; $P > 0.05$).

To quantify muscle spindle group Ia innervation, the muscle spindles from nondiabetic mice were visualized on a confocal microscope, and two axonal parameters were measured: axonal width and IRD, defined as the distance between the Ia axonal annulospiral rotations. Within the nondiabetic group of mice, there was a mean axonal width of 1.3 μm with very low variability (±0.19 SD) and a mean IRD of 3.6 μm with low variability (±0.98). Up to 12 muscle spindles can be found within one mouse gastrocnemius muscle, and the mean axonal width and IRD were very consistent not only overall in the nondiabetic group, but also within individual muscles (Fig. 2*A–D*). These results indicate that within nondiabetic muscle spindles there is a high degree of homogeneity in axonal width and IRD.

Axonal width and IRD were also measured in muscle spindles from diabetic mice. The mean axonal width of diabetic mice (mean ± SD, 1.3 ± 0.42 μm) was not significantly different from that of nondiabetic mice ($P > 0.05$). In addition, the mean IRD of diabetic mice (3.9 ± 1.59 μm) was not significantly different from that of nondiabetic mice ($P > 0.05$). However, a clear pattern began to appear when analyzing the values for the two spindle parameters in diabetic and nondiabetic mice. As described above, the nondiabetic mice had reliable consistency with each spindle parameter within their group and within individual muscles. In contrast, this consistency

TABLE 2
Footprinting, gridwalking, and rotorod tests failed to detect sensorimotor deficits in C57BL/6 diabetic mice

	Nondiabetic	Diabetic
Footprinting		
n	5	5
Step length	8.5 ± 0.20	7.7 ± 0.43
Toe spread	0.8 ± 0.05	0.7 ± 0.02
Inter-toe spread	0.3 ± 0.01	0.3 ± 0.03
Print length	0.7 ± 0.04	0.7 ± 0.03
Gridwalking		
n	3	3
	0.7 ± 0.19	0.9 ± 0.46
Rotorod latency		
n	5	5
	172 ± 60.3	222 ± 51.0

Data are means ± SEM. Results from three behavioral tasks at 9–10 weeks post-STZ injection in C57BL/6 mice. Footprinting parameters included step length, toe spread (toes 1–5), inter-toe spread (toes 2–4), and print length, and these analyses did not detect differences between nondiabetic and diabetic mice ($P > 0.05$). Likewise, the grid walk did not detect a difference in the percentage of slips between diabetic and nondiabetic mice ($P > 0.05$). Diabetic mice had a similar latency on the rotorod compared with nondiabetic mice ($P > 0.05$). Footprinting parameters are in centimeters; gridwalking is the % slips in 5 min on the grid; rotorod latency is in seconds.

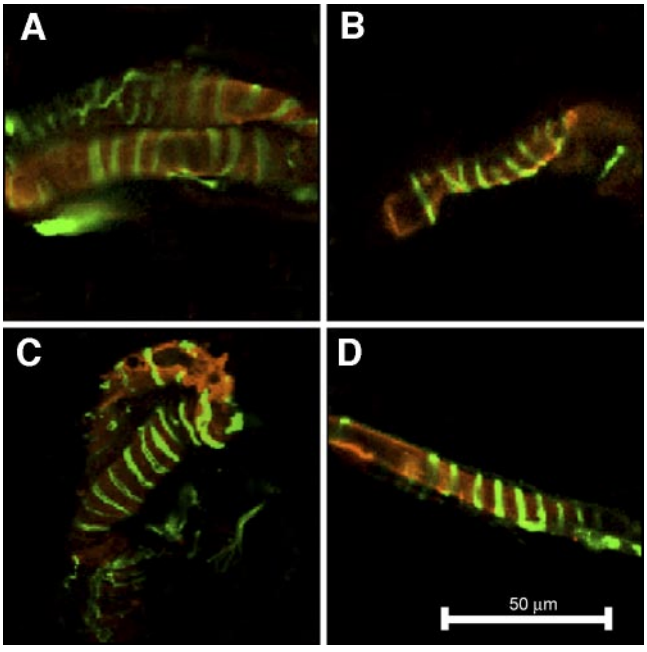

FIG. 2. Typical muscle spindle Ia innervation in nondiabetic C57BL/6 mice. Confocal optical images from the equatorial region of medial gastrocnemius muscle spindles from a nondiabetic mouse (*A* and *B*) illustrate consistent axonal width and IRD within one muscle. In addition, spindles from two other nondiabetic mice (*C* and *D*) display similar consistency in axonal width and IRD, reflective of all nondiabetic animals. Red visualizes slow tonic myosin heavy chain (S46) expression within spindle bag fibers, and green represents NF-H–positive Ia axons with their characteristic annulospiral morphology.

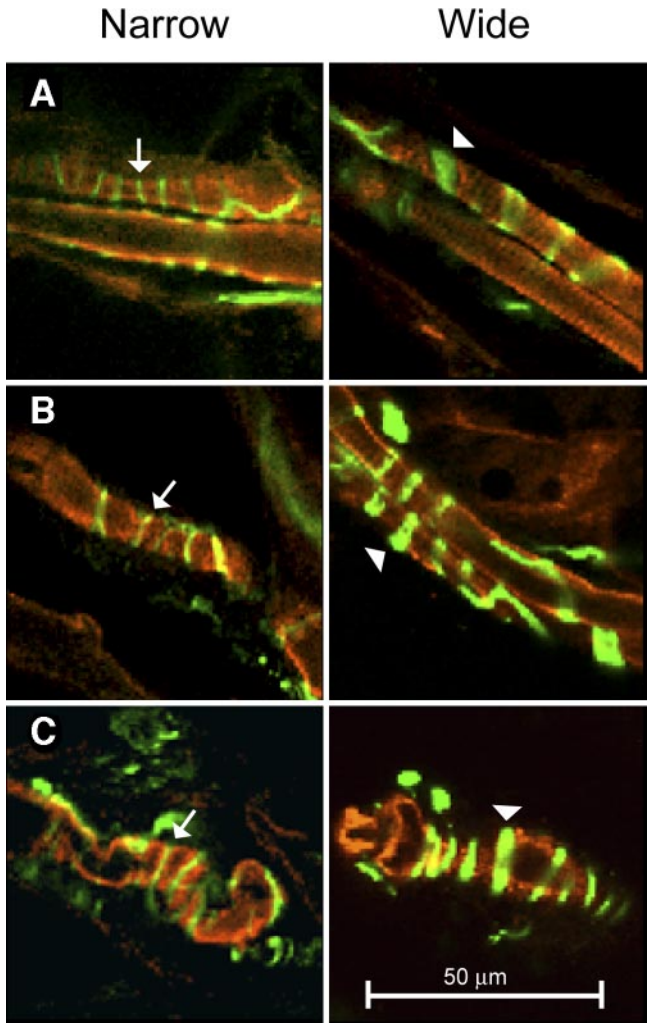

FIG. 3. Altered muscle spindle Ia innervation in diabetic C57BL/6 mice. Confocal optical images from the equatorial region of medial gastrocnemius muscle spindles from diabetic mice (*A*, *B*, and *C*) show that within one diabetic muscle, both thinner and thicker axons are evident. These images highlight the variability in diabetic muscle spindle innervation morphology. Red visualizes slow tonic myosin heavy chain (S46) expression within spindle bag fibers, and green represents NF-H–positive Ia axons with their characteristic annulospiral morphology. The white arrows denote very thin axons and the white arrowheads denote very thick axons.

was not seen in the diabetic mice. Multiple distinct and abnormal morphologies were identified in diabetic mice, resulting in a high degree of variability. In diabetic mice, the mean axonal width of Ia axons was sometimes more narrow, sometimes wider, or sometimes average compared with those in nondiabetic mice (Fig. 3*A–C* and Fig. 4*A*). Axonal width in nondiabetic mice ranged from only 0.9 to 1.6 μm, whereas axonal width in diabetic mice ranged from 0.8 to 2.6 μm. Similarly, Ia axons in the diabetic mice sometimes had smaller IRDs (axon rotations closer together), sometimes larger IRDs (axon rotations further apart), or sometimes average IRDs compared with those in the nondiabetic mice (Fig. 4*B*). IRD in nondiabetic mice ranged from only 1.3 to 6.0 μm, whereas IRD in diabetic mice ranged from 1.2 to 8.2 μm. Although the size difference for small IRDs was minimal (1.2–1.3 μm), many diabetic animals displayed this small phenotype. Axonal width and IRD were variable not only between animals of the diabetic group (Fig. 4*A* and *B*) but also within muscles of individual animals. The coefficient of variation (CoV) was calculated [CoV (%) = SD/mean × 100] for each diabetic and nondiabetic muscle as a marker of variability. For axonal width, diabetic mice had a mean CoV of 30.8%, which is five times more variable than that of nondiabetic mice (6.5%) (Fig. 4*C*). For IRD, the CoV of diabetic mice (36.1%) was 1.5 times more variable than that of nondiabetic mice (CoV 24.5%) (Fig. 4*D*). Overall, these results suggest that diabetic muscle spindle Ia fibers have high variability in their axonal width and IRD as a group and within individual muscle spindles.

Muscle spindles from db^+ and *db/db* mice were analyzed to determine whether Ia axon variability observed in the STZ-induced type 1 diabetic mice was also present in a type 2 diabetes model. There was no difference in axonal width between db^+ and *db/db* mice (data not shown). However, similar to STZ-induced C57BL/6 diabetic mice, *db/db* mice displayed a high degree of variability in their mean IRDs compared with db^+ mice. Ia axons in *db/db* mice sometimes had smaller IRDs, sometimes larger IRDs, or sometimes average IRDs compared with db^+ mice (Fig. 5*A–C*). IRD in db^+ mice ranged from 1.4 to 3.5 μm, where IRD in *db/db* mice ranged from 1.2 to 9.0 μm (Fig. 5*D*). This indicates that *db/db* mice display greater variability in their IRDs than db^+ mice, suggesting that alterations in Ia axon morphology occur in both type 1 and type 2 diabetes models of DPN.

Insulin replacement therapy was administered to determine whether the behavioral and anatomical changes in STZ-induced diabetic mice were reversible. At 1 and 5 weeks post-STZ injection, no significant differences in beam-walk slips were apparent between nondiabetic, diabetic, and diabetic + insulin mice ($P > 0.05$; Fig. 6*A*). However, after 10 weeks post-STZ, the diabetic mice

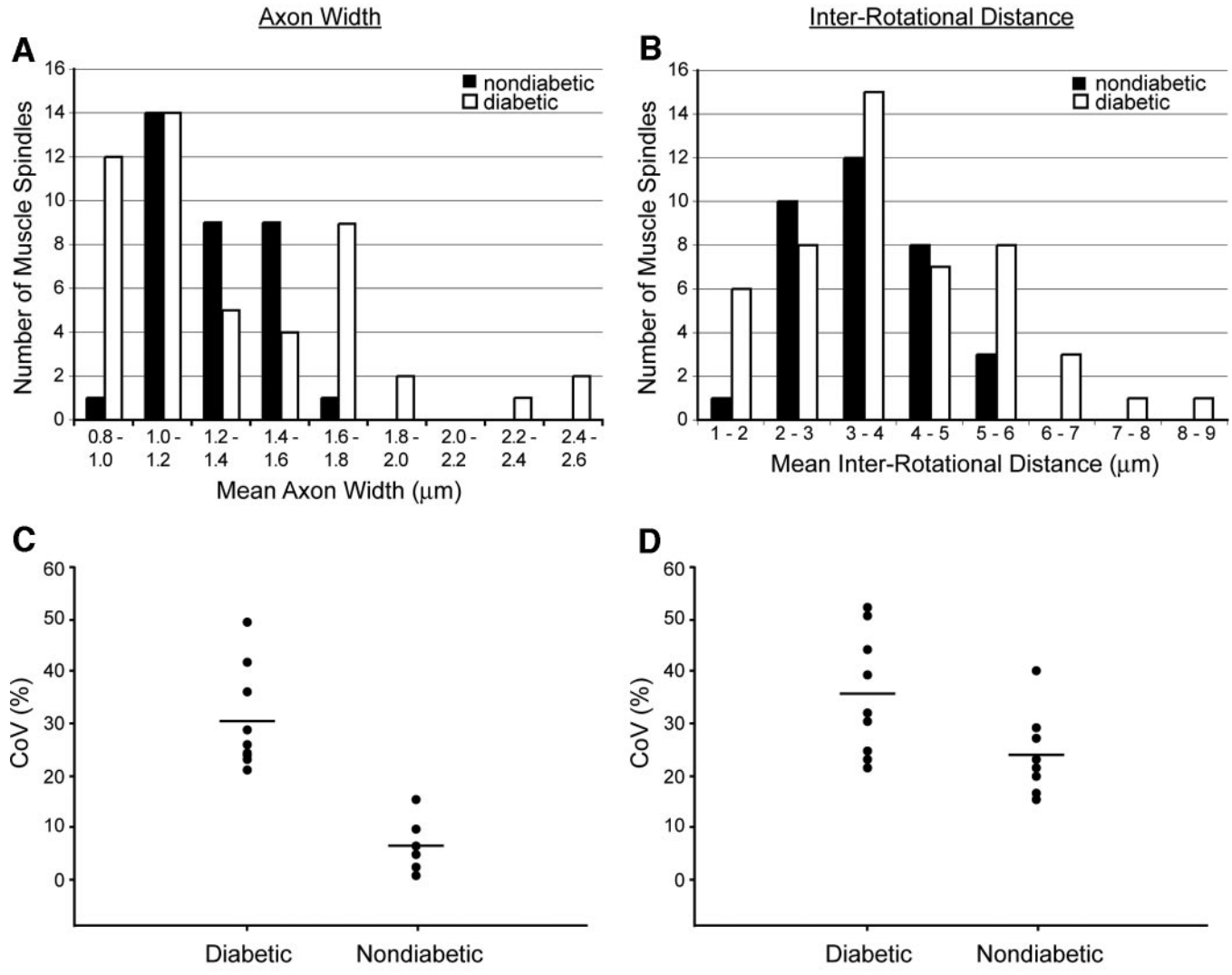

FIG. 4. Ia axonal width and IRD in diabetic and nondiabetic C57BL/6 mice. *A*: Mean axonal width was more variable in diabetic mice ($n = 10$) compared with nondiabetic mice ($n = 8$). Nondiabetic mice have a tighter range of widths than diabetic mice. The variability in diabetic mice is also higher for IRD (*B*), where nondiabetic mice have a tighter range of IRDs than diabetic mice. Note that there are increased numbers of smaller or larger Ia axons in diabetic compared with nondiabetic mice (*A*), and there are rotations that are spaced closer together or further apart in diabetic compared with nondiabetic mice (*B*). Diabetic mice have increased variability in axonal width in muscles of individual animals compared with nondiabetic mice (*C*). Diabetic mice also have increased variability in IRD in individual muscles compared with nondiabetic mice (*D*). CoV, coefficient of variation. Black circles represent one muscle, and black lines represent the mean coefficient of variation in each group (*C* and *D*).

displayed significantly more slips (1.2 ± 0.07) than nondiabetic mice (0.5 ± 0.20, $P = 0.05$), as shown previously. Importantly, diabetic mice treated with insulin improved their beam performance and had significantly fewer slips (0.3 ± 0.07) than diabetic mice with sham pellets ($P < 0.05$) and were not significantly different than nondiabetic mice ($P > 0.05$; Fig. 6*A*).

Axonal width and IRD were also measured in muscle spindles from diabetic versus diabetic + insulin mice. The multiple axonal morphologies previously identified in diabetic mice that resulted in a high degree of variability were reversed in insulin-treated diabetic mice. In diabetic + insulin mice, the mean axonal width of Ia axons was more consistent than in diabetic mice and was comparable with that in nondiabetic mice (Fig. 6*B*). Axonal width in diabetic + insulin mice ranged from only 0.9 to 2.0 μm, whereas axonal width in diabetic mice ranged from 0.8 to 2.9 μm. Similarly, IRD variability was decreased in diabetic + insulin mice (Fig. 6*C*). IRD in diabetic + insulin mice ranged from only 1.6 to 4.0 μm, whereas IRD in diabetic mice ranged from 1.2 to 8.0 μm.

Not only was axonal width and IRD variability decreased overall in insulin-treated mice, but also within muscles of individual animals. For axonal width, diabetic mice had a mean CoV of 44.4%, which is 2.5 times more variable than that of diabetic + insulin mice (18.0%; Fig. 6*D*). For IRD, the CoV of diabetic mice also indicated about two times more variability (37.4%) than that of diabetic + insulin mice (17.6%; Fig. 6*E*).

DISCUSSION

In this study, type 1 and type 2 mouse models of diabetes were used to examine large-fiber diabetic sensorimotor polyneuropathy. Our results reveal that STZ-induced diabetes leads to sensorimotor behavioral deficits involving balance and gait detectable by the beam-walk apparatus. These behavioral abnormalities are hypothesized to be a

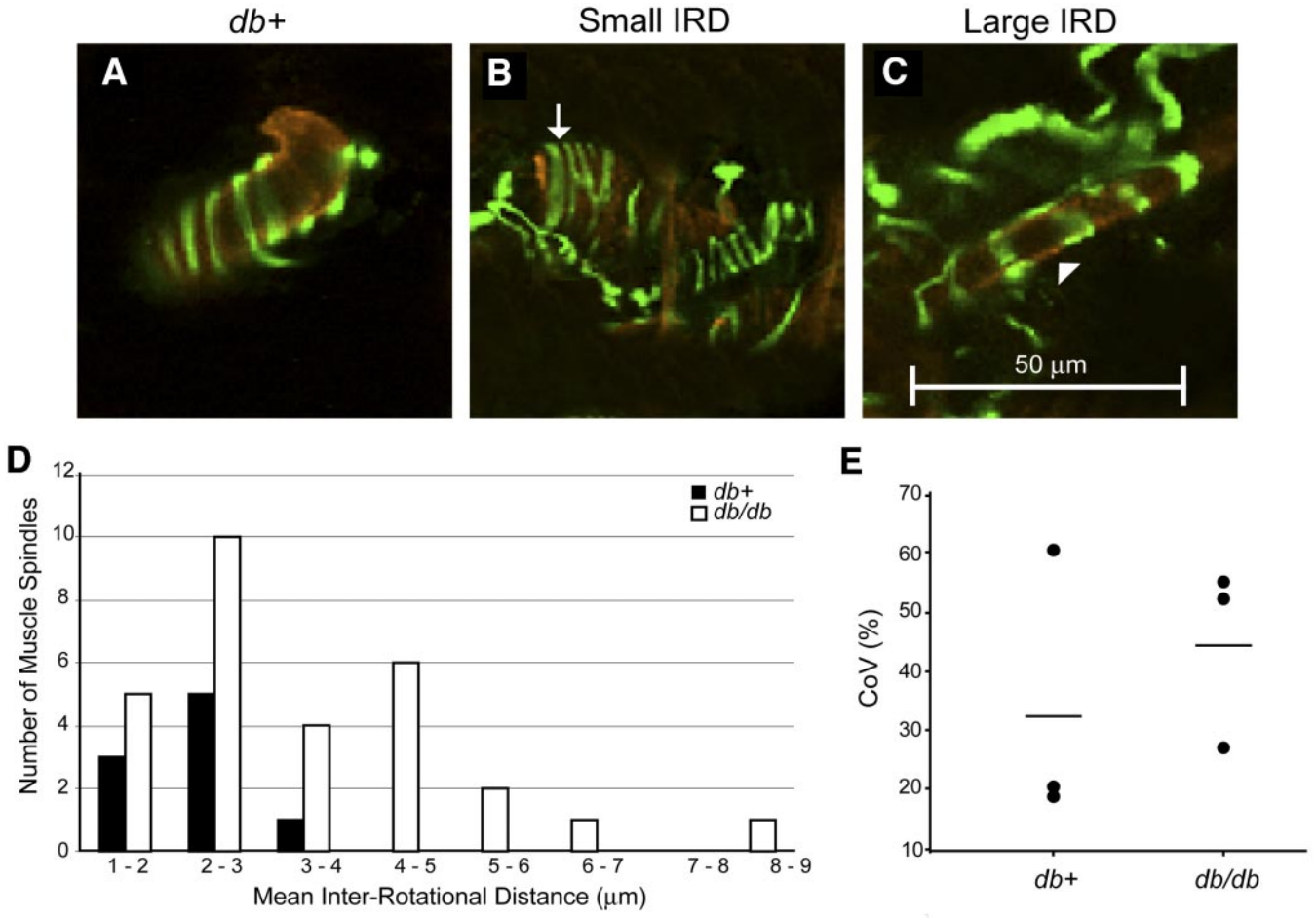

FIG. 5. Variable IRD in *db/db* and *db*$^+$ mice. Confocal optical images from the equatorial region of medial gastrocnemius muscle spindles from a *db*$^+$ mouse showing the average IRD in the control mice (*A*). IRD values from *db/db* mice ranged from being smaller than *db*$^+$ IRD to being much larger than *db*$^+$ IRD (*B* and *C*). These images highlight the variability in *db/db* muscle spindle innervation morphology. Red visualizes slow tonic myosin heavy chain (S46) expression within spindle bag fibers, and green represents NF-H–positive Ia axons with their characteristic annulospiral morphology. The white arrow denotes small IRDs, and the white arrowhead denotes large IRDs. IRD was more variable in diabetic than in nondiabetic mice (*D*). *db/db* mice displayed an increased variability in IRD in muscles of individual animals compared with *db*$^+$ mice (*E*). CoV, coefficient of variation. Black circles represent one muscle, and black lines represent the mean coefficient of variation in each group (*E*).

consequence of the irregularities and variability in muscle spindle group Ia innervation. In addition, similar alterations in innervation were identified in a type 2 diabetes mouse model. Collectively, these results suggest that diabetic mice undergo damage to large sensory axons that may contribute to deficits in large-fiber sensory feedback associated with balance and gait. Importantly, insulin treatment of STZ-induced diabetic mice effectively reversed these behavioral and anatomical deficits, supporting the view that these abnormalities were a result of diabetes and are sensitive to insulin therapy.

The beam-walk apparatus has been used to assess sensorimotor deficits following brain injury and other conditions resulting in altered gait, balance, and/or proprioception (21–23). Baskin et al. (24) suggested that the beam-walk task is effective in detecting sensorimotor deficits resulting primarily from hindlimb dysfunction. In previous studies, we have used the beam-walk apparatus to evaluate sensorimotor function in relation to hindlimb muscle spindle innervation, and the performance of mice using this approach reliably mirrored the reinnervation of muscle spindles following nerve crush (17). Importantly, the beam-walk apparatus was found to be the most sensitive measure for diabetes-induced sensorimotor changes, as footprinting, the grid-walk, and rotorod were not able to detect altered behavior. However, it is noted that more sophisticated measures of gait analysis may reveal deficits that footprinting with ink could not. In addition, the sensorimotor changes observed in the diabetic mice were subtle, suggesting that the beam may challenge the mice to rely on sensorimotor feedback more so than the other tasks discussed above.

SNCV has been widely studied in rodent models of diabetic neuropathy, and it is thought that slowed conduction velocities likely reflect deficits in conduction predominantly in large nerve fibers. However, reports of diabetes-induced slowed SNCV can be variable, with some studies reporting decreases (25), while others report no change (26). This may be due to inherent animal model differences, just as some models display cutaneous insensitivity while others report allodynia. Our studies revealed no reductions in SNCV in STZ-induced diabetic mice; however, we did detect decreases in MNCV. It is not surprising that our model did not have decreased SNCV simply due to the subtle large-fiber morphologic alterations in which, perhaps, some fibers compensate for others while in different states of flux. It is plausible to predict that rodents with significantly slowed SNCV may have a more severe phenotype related to spindle innervation.

Typically, muscle spindle quantification has involved

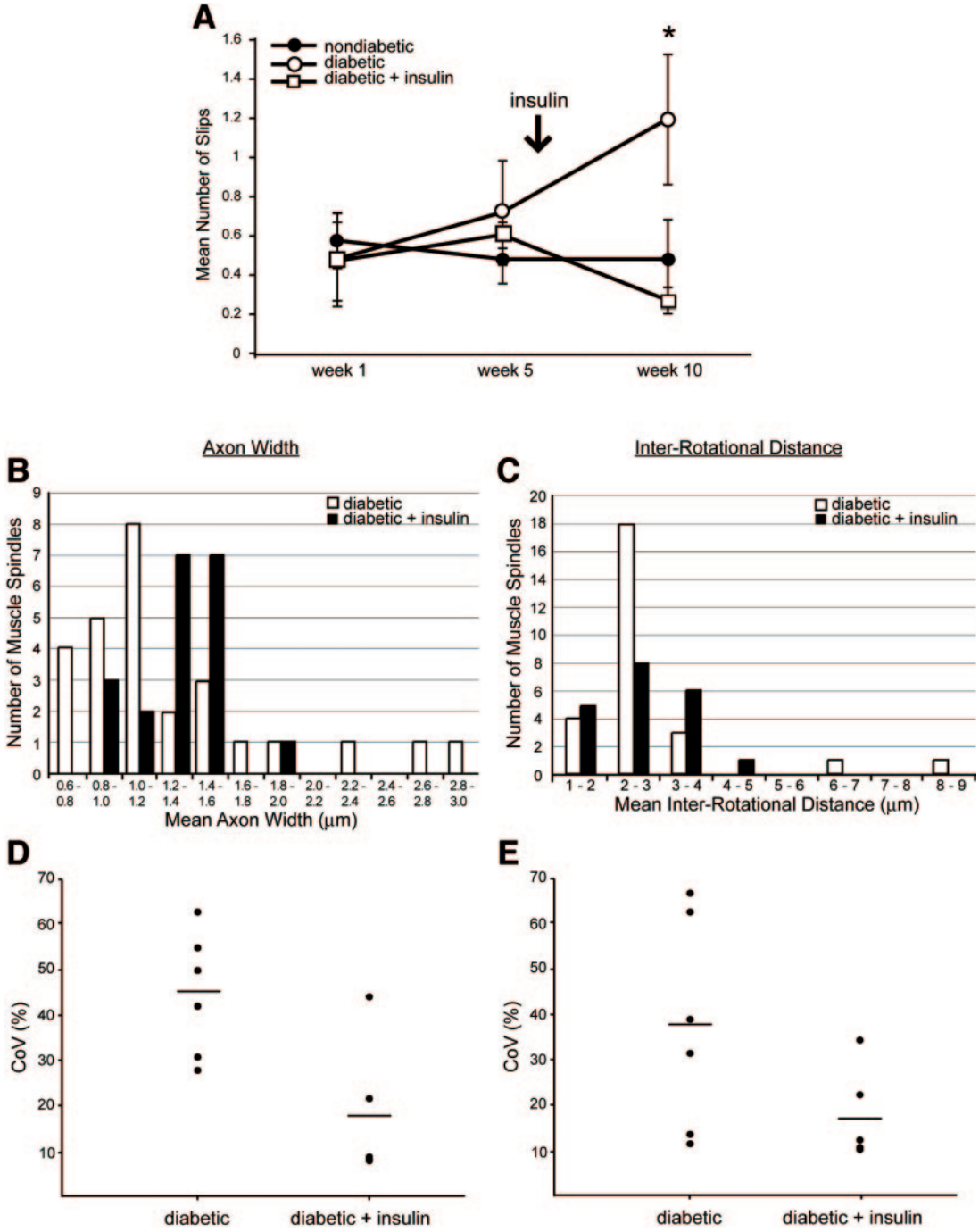

FIG. 6. Insulin treatment repairs sensorimotor behavioral deficits and altered muscle spindle innervation in diabetic C57BL/6 mice. *A*: Quantification of mean hindpaw footslips for nondiabetic ($n = 6$), diabetic ($n = 6$), and diabetic + insulin ($n = 5$) mice at 1, 5, and 10 weeks' post-STZ injection. Arrow denotes time of insulin pellet administration at 6 weeks post-STZ. Data are presented as means ± SEM. *$P \leq 0.05$ diabetic vs. nondiabetic and diabetic vs. diabetic + insulin. *B*: Mean axonal width was less variable with a tighter range in diabetic + insulin treated mice compared with diabetic mice with sham pellets. The variability in diabetic + insulin mice is also lower for IRD (*C*). Diabetic + insulin mice also decreased their variability in axonal width and IRD in muscles of individual animals compared with diabetic mice (*D* and *E*). CoV, coefficient of variation. Black circles represent one muscle, and black lines represent the mean coefficient of variation in each group (*D* and *E*).

cross sections of the spindle capsule through light or electron microscopy (15,27–29). This method of visualizing the spindle does not allow for intricate analysis of axon morphology. Visualizing muscle spindle afferents longitudinally provides more information about axonal width and IRD. To our knowledge, our study is the first to quantify Ia annulospiral endings on muscle spindle intrafusal fibers in diabetic mice, and this technique now provides a new assay to determine the efficacy of therapeutic interventions aimed at improving large-fiber diabetic neuropathy. Small-fiber neuropathy has benefited greatly from quantitative assessments in epidermal innervation, and an analogous approach has been lacking for large fibers. In addition, it is difficult to access spindle innervation in human muscle biopsies, reinforcing the need for animal model studies to address the pathogenesis and treatment of human large-fiber DPN.

Fiber changes commonly reported in DPN include ax-

onal degeneration, regeneration, demyelination, and remyelination (30). A study examined muscle spindles in STZ-treated diabetic rats and reported axonal dilation and axonal dystrophy (31). Using electron microscopy analysis, diabetic rats revealed enlarged sciatic nerve axon terminals, intrafusal fiber nuclear disintegration, and increased numbers of Schwann cells, all suggestive of degeneration and regeneration (31). This study is consistent with our more detailed observations of thicker, thinner, closer-spaced, and further-spaced axons and supports the proposed view that Ia axons undergo degeneration and subsequent regeneration in diabetic mice.

It is plausible that extrafusal fiber atrophy could drive changes in spindle innervation. Although muscle wasting was not measured here, it is likely that muscle wasting occurs in STZ-induced diabetic mice. It may be worthwhile to assess spindle innervation in other muscle wasting diseases such as muscular dystrophy or myasthenia gravis. In human muscle spindles from patients with Duchenne muscular dystrophy, changes were apparent in capsule thickness and intrafusal fiber number and diameter (32). No measures of quantifiable spindle innervation were documented; however, certain spindles were reported to be devoid of axons.

Likewise, it is possible that changes in intrafusal bag fibers may influence Ia axon innervation. Bag fibers are enlarged in the equatorial region due to the accumulation of nuclei, and this variability makes it difficult to measure intrafusal fiber size. However, our observations suggest that some intrafusal fibers in diabetic mice appeared abnormal (Fig. 3*C*), and it is reasonable to suggest that annulospiral innervation is influenced by intrafusal fiber morphology.

Irrespective of the cause leading to altered annulospiral morphology, a plausible outcome of abnormal Ia afferent innervation may be altered electrophysiological output from spindles. Muscle spindle afferent axons fire when the extrafusal fiber and subsequent intrafusal fibers stretch, leading to increased activity of the Ia axon. It is reasonable to suggest that when Ia axon morphology is disrupted, it leads to changes in the firing patterns of the spindle afferent. Collectively, the varied Ia innervation in spindles from diabetic mice could lead to changes in overall Ia firing patterns and result in asynchronous Ia firing within diabetic muscles. Furthermore, this variation in sensory input could affect motor neuron function as well.

Our results reveal that both axonal width and IRD were varied in STZ-induced diabetic compared with nondiabetic mice. However, in the type 2 diabetes mouse model, only IRD varied in the *db/db* but not db^+ mice. The difference between *db/db* and STZ-induced diabetes may be related to the severity of neuropathy in the type 2 diabetes model or the rate of progression of the neuropathy. It is possible that altered IRD is the first sign of axonal damage and precedes variability in axonal width.

In conclusion, we have identified reversible behavioral and pathological large sensory nerve fiber–related changes in diabetic mice. Future studies should address treatment paradigms to repair muscle spindle afferent innervation and consequently improve sensorimotor function. These studies will provide new insight into the treatment and prevention of large-fiber complications that develop in humans suffering from diabetes.

ACKNOWLEDGMENTS

Support was contributed by National Institutes of Health Grant R01NS43314 (to D.E.W.), the Juvenile Diabetes Research Foundation (to D.E.W. and E.L.F.), and the Biomedical Research Training Program at the University of Kansas Medical Center (to K.A.M.).

Some data from this study was previously presented in poster form at the 36th annual meeting of the Society for Neuroscience Atlanta, Georgia, 14–18 October 2006.

The authors thank Megan Johnson for helpful comments on the manuscript, Dr. Frank Stockdale for the anti-S46 antibody, Gregory Onyszchuk and Jason Ryals for assistance with development and production of the grid-walk apparatus, James McBride and Rick Debrowsky for assistance with electrophysiology, and members of the Wright laboratory for helpful discussions.

REFERENCES

1. Duby JJ, Campbell RK, Setter SM, White JR, Rasmussen KA: Diabetic neuropathy: an intensive review. *AM J Health-Syst Pharm* 61:160–176, 2004
2. Drel VR, Mashtalir N, Ilnytska O, Shin J, Li F, Lyzogubov VV, Obrosova IG: The leptin-deficient (ob/ob) mouse: a new animal model of peripheral neuropathy of type 2 diabetes and obesity. *Diabetes* 55:3335–3343, 2006
3. Johnson MS, Ryals JM, Wright DE: Diabetes-induced chemogenic hypoalgesia is paralleled by attenuated stimulus-induced Fos expression in the spinal cord of diabetic mice. *J Pain* 8:637–649, 2007
4. Sullivan KA, Hayes JM, Wiggin TD, Backus C, Su Oh S, Lentz SI, Brosius F 3rd, Feldman EL: Mouse models of diabetic neuropathy. *Neurobiol Dis* 28:276–285, 2007
5. Calcutt NA, Jorge MC, Yaksh TL, Chaplan SR: Tactile allodynia and formalin hyperalgesia in streptozotocin-diabetic rats: effects of insulin, aldose reductase inhibition and lidocaine. *Pain* 68:293–299, 1996
6. Casellini CM, Vinik AI: Clinical manifestations and current treatment options for diabetic neuropathies. *Endocr Pract* 13:550–566, 2007
7. Cavanagh PR, Derr JA, Ulbrecht JS, Maser RE, Orchard TJ: Problems with gait and posture in neuropathic patients with insulin-dependent diabetes mellitus. *Diabet Med* 9:469–474, 1992
8. Uccioli L, Giacomini PG, Monticone G, Magrini A, Durola L, Bruno E, Parisi L, Di Girolamo S, Menzinger G: Body sway in diabetic neuropathy. *Diabetes Care* 18:339–344, 1995
9. Richardson JK, Sandman D, Vela S: A focused exercise regimen improves clinical measures of balance in patients with peripheral neuropathy. *Arch Phys Med Rehabil* 82:205–209, 2001
10. Nardone A, Galante M, Pareyson D, Schieppati M: Balance control in sensory neuron disease. *Clin Neurophysiol* 118:538–550, 2007
11. Stapley PJ, Ting LH, Hulliger M, Macpherson JM: Automatic postural responses are delayed by pyridoxine-induced somatosensory loss. *J Neurosci* 22:5803–5807, 2002
12. Waxman SG: *Lange Clinical Neuroanatomy.* 25th ed. New York, McGraw-Hill, 2003
13. Swash M, Fox KP: The effect of age on human skeletal muscle: studies of the morphology and innervation of muscle spindles. *J Neurol Sci* 16:417–432, 1972
14. Kararizou E, Manta P, Kalfakis N, Vassilopoulos D: Morphometric study of the human muscle spindle. *Anal Quant Cytol Histol* 27:1–4, 2005
15. Chen HH, Tourtellotte WG, Frank E: Muscle spindle-derived neurotrophin 3 regulates synaptic connectivity between muscle sensory and motor neurons. *J Neurosci* 22:3512–3519, 2002
16. Wang ZC, Dohle JF, Friemann J, Green BS: Prevention of high- and low-dose STZ-induced diabetes with d-glucose and 5-thio-d-glucose. *Diabetes* 42:420–428, 1993
17. Taylor MD, Holdeman AS, Weltmer SG, Ryals JM, Wright DE: Modulation of muscle spindle innervation by neurotrophin-3 following nerve injury. *Exp Neurol* 191:211–222, 2005
18. Taylor MD, Vancura R, Williams JM, Riekhof JT, Taylor BK, Wright DE: Overexpression of neurotrophin-3 in skeletal muscle alters normal and injury-induced limb control. *Somatosens Mot Res* 18:286–294, 2001
19. Onyszchuk G, Al-Hafez B, He YY, Bilgen M, Berman NE, Brooks WM: A mouse model of sensorimotor controlled cortical impact: characterization using longitudinal magnetic resonance imaging, behavioral assessments, and histology. *J Neurosci Methods* 160:187–196, 2007
20. Stevens MJ, Obrosova I, Cao X, Van Huysen C, Greene DA: Effects of

DL-alpha-lipoic acid on peripheral nerve conduction, blood flow, energy metabolism, and oxidative stress in experimental diabetic neuropathy. *Diabetes* 49:1006–1015, 2000
21. Fox GB, Fan L, Levasseur RA, Faden AI: Sustained sensory/motor and cognitive deficits with neuronal apoptosis following controlled cortical impact brain injury in the mouse. *J Neurotrauma* 15:599–614, 1998
22. Sherbel U, Raghupathi R, Nakamura M, Saatman KE, Trojanowski JQ, Neugebaumer E, Marino MW, McIntosh TK: Differential acute and chronic responses of tumor necrosis factor-deficient mice to experimental brain injury. *Proc Natl Acad Sci U S A* 96:8721–8726, 1999
23. Ferrer I, Kapfhammer JP, Hindelang C, Kemp S, Troffer-Charlier N, Broccoli V, Callyzot N, Mooyer P, Selhorst J, Vreken P, Wanders RJ, Mandel JL, Pujol A: Inactivation of the peroxisomal ABCD2 transporter in the mouse leads to late-onset ataxia involving mitochondria, Golgi and endoplasmic reticulum damage. *Hum Mol Genet* 14:3565–3577, 2005
24. Baskin YK, Dietrich WD, Green EJ: Two effective behavioral tasks for evaluating sensorimotor dysfunction following traumatic brain injury in mice. *J Neurosci Methods* 129:97–93, 2003
25. Mizisin AP, Calcutt NA, Tomlinson DR, Gallagher A, Fernyhough P: Neurotrophin-3 reverses nerve conduction velocity deficits in streptozotocin-diabetic rats. *J Peripher Nerv Syst* 4:211–221, 1999
26. Jefferys JG, Brismar T: Analysis of peripheral nerve function in streptozotocin diabetic rats. *J Neurol Sci* 48:435–444, 1980
27. Wang J, McWhorter DL, Walro JM: Stability of myosin heavy chain isoforms in selectively denervated adult rat muscle spindles. *Anat Rec* 249:32–43, 1997
28. Wright DE, Zhou L, Kucera J, Snider WD: Introduction of a neurotrophin-3 transgene into muscle selectively rescues proprioceptive neurons in mice lacking endogenous neurotrophin-3. *Neuron* 19:503–517, 1997
29. Chen XJ, Levedakou EN, Millen KJ, Wollmann RL, Soliven B, Popko B: Proprioceptive sensory neuropathy in mice with a mutation in the cytoplasmic dynein heavy chain 1 gene. *J Neurosci* 27:14515–14524, 2007
30. Sinnreich M, Taylor BV, Dyck PJB: Diabetic neuropathies: classification, clinical features, and pathophysiological basis. *Neurologist* 11:63–79, 2005
31. Weis J, Dimpfel W, Schroder JM: Nerve conduction changes and fine structural alterations of extra- and intrafusal muscle and nerve fibers in streptozotocin diabetic rats. *Muscle Nerve* 18:175–184, 1995
32. Swash M, Fox KP: The pathology of the muscle spindle in Duchenne muscular dystrophy. *J Neurol Sci* 29:17–32, 1976